CHEMISTRY OF MATERIALS
Cite This: Chem. Mater. 2018, 30, 5315−5321
Article
pubs.acs.org/cm

Optical, Electronic, and Magnetic Engineering of ⟨111⟩ Layered Halide Perovskites

Brenda Vargas,[†,▲] Raúl Torres-Cadena,[†,▲] Joelis Rodríguez-Hernández,[‡] Milan Gembicky,[§] Haomiao Xie,[∥] José Jiménez-Mier,[⊥] Yi-Sheng Liu,[#] Eduardo Menéndez-Proupin,[¶] Kim R. Dunbar,[∥] Nazario Lopez,[●] Paul Olalde-Velasco,*[,■] and Diego Solis-Ibarra*[,†]

[†]Laboratorio de Fisicoquímica y Reactividad de Superficies (LaFReS), Instituto de Investigaciones en Materiales, Universidad Nacional Autónoma de México, CU, Coyoacán, 04510, Ciudad de México, México

[‡]Centro de Investigación en Química Aplicada (CIQA), Blvd. Enrique Reyna Hermosillo, No. 140, Saltillo, Coahuila 25294, México

[§]Department of Chemistry and Biochemistry, University of California, San Diego, 9500 Gilman Drive, La Jolla, California 92093, United States

[∥]Department of Chemistry, Texas A&M University, College Station, Texas 77845, United States

[⊥]Instituto de Ciencias Nucleares, Universidad Nacional Autónoma de México, CU, Coyoacán, 04510, Ciudad de México, México

[#]Advanced Light Source, Lawrence Berkeley National Laboratory, Berkeley, California 94720, United States

[¶]Grupo de Modelación de Materiales, Departamento de Física, Facultad de Ciencias, Universidad de Chile, Las Palmeras, 3425, Ñuñoa 780-0003, Santiago, Chile

[●]Centro de Investigaciones Químicas, IICBA, Universidad Autónoma del Estado de Morelos, Av. Universidad 1001, Col. Chamilpa, Cuernavaca, Morelos 62209, México

[■]Instituto de Física, Benemérita Universidad Autónoma de Puebla, Apdo. Postal J-48, Puebla, Puebla 72570, México

Supporting Information

ABSTRACT: Antimony and bismuth ⟨111⟩ layered perovskites have recently attracted significant attention as possible, nontoxic alternatives to lead halide perovskites. Unlike lead halide perovskites, however, ⟨111⟩ halide perovskites have shown limited ability to tune their optical and electronic properties. Herein, we report on the metal alloying of manganese and copper into the family of materials with formula $Cs_4Mn_{1-x}Cu_xSb_2Cl_{12}$ (x = 0−1). By changing the concentration of manganese and copper, we show the ability to modulate the bandgap of this family of compounds over the span of 2 electron volts, from 3.0 to 1.0 eV. Furthermore, we show that in doing so, we can also adjust other relevant properties such as their magnetic behavior and their electronic structure.

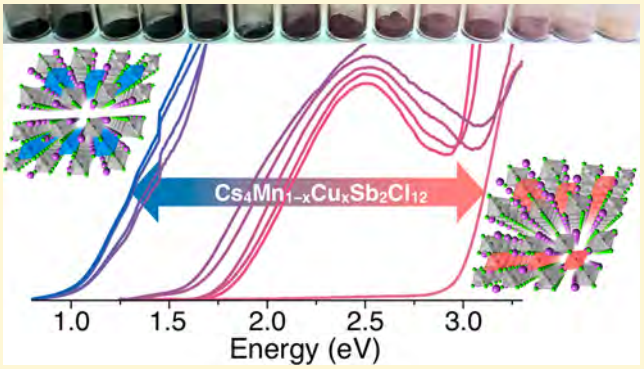

INTRODUCTION

Three-dimensional (3D) perovskites and ⟨100⟩ layered perovskites have been extensively investigated as absorbers in solar cells and have had great success when incorporated into optoelectronic devices. One of the key properties that have allowed them to thrive in the field of optoelectronics is their ability to fine-tune their optical properties (i.e., bandgap and photoluminescence).[1−4] This has been accomplished mainly by changing or mixing different halides (Cl, Br, and I) and to a lesser degree, by mixing A site cations (i.e., methylammonium, formamidinium, and/or cesium) or the B metals (i.e., tin or germanium).[1]

Recently, we[5] and others[6,7] have reported on the promising properties and applications of a relatively unknown family of perovskites, known as ⟨111⟩ layered perovskites. While relatively new in the field of optoelectronics, in a couple of years, ⟨111⟩ perovskites have achieved power conversions efficiencies of up to 1.5%, while increasing the overall stability and decreasing the toxicity by virtue of replacing lead with metals such as bismuth and antimony.[6,8−12] Unlike other halide perovskites, ⟨111⟩ halide perovskites do not need a metal, or combination of metals with a 2+ overall charge, which allows for the incorporation of other nontoxic elements such as bismuth, antimony, and copper.[5,7] Despite significant

Received: May 17, 2018
Revised: July 12, 2018
Published: July 13, 2018

DOI: 10.1021/acs.chemmater.8b02099
Chem. Mater. 2018, 30, 5315−5321

advances in the field, and in contrast to lead halide perovskites, up to date, there has been very limited progress modulating the optical and electronic properties of ⟨111⟩ halide perovskites, double perovskites, or even ⟨110⟩ perovskites for that matter.[2] Herein, we report on the synthesis and characterization of a new family of materials with formulas $Cs_4Mn_{1-x}Cu_xSb_2Cl_{12}$, where x ranges from 0 to 1. By systematically changing the manganese to copper ratio, we show that it is possible to modulate the optical bandgap of these materials from 1.0 to 2.9 eV. Furthermore, we show that their magnetic properties and electronic structure can also be tuned by the same means.

RESULTS AND DISCUSSION

Synthetic Aspects. This family of materials, $Cs_4Mn_{1-x}Cu_xSb_2Cl_{12}$, can be synthesized in large quantities and good yields (>85%) by adding CsCl to a solution of Sb_2O_3, $MnCl_2$, and/or $CuCl_2$ in concentrated hydrochloric acid. Alternatively, $Cs_4Mn_{1-x}Cu_xSb_2Cl_{12}$ can be obtained by a solid-state reaction at 400 °C between $Cs_4MnSb_2Cl_{12}$ and $Cs_4CuSb_2Cl_{12}$ in the desired stoichiometry (see Supporting Information (SI) for details). The stoichiometry of the obtained materials was corroborated by energy-dispersive X-ray spectroscopy (EDS, Table S3 and Figure S1), which showed that regardless of the method and the Mn:Cu ratio, the composition of the final materials almost perfectly matched that of the desired stoichiometry. The fact that this family of mixed-metal materials allows for full solubility with x values covering the entire range between 0 and 1 is remarkable by itself, especially when considering the distinct geometrical preferences of these two metal ions.[13]

Single crystals of the Mn-only structure were obtained by slow cooling a concentrated solution of $Cs_4MnSb_2Cl_{12}$ in concentrated HCl (see SI for details). Single crystal X-ray diffraction (SCXRD) studies of such crystals determined that $Cs_4MnSb_2Cl_{12}$ crystallizes in a trigonal $R\bar{3}m$ space group. Like the Cu-only ($Cs_4CuSb_2Cl_{12}$) structure, the Mn-only structure is a ⟨111⟩-oriented triple-layered (n = 3) perovskite of alternating corner sharing $MnCl_6$ and $SbCl_6$ octahedra (Figure 1A). Unlike the copper atom in the Cu-only structure, the manganese forms perfect $MnCl_6$ octahedra in the Mn-only structure with Mn−Cl distances of 2.522 (1) Å. The lack of distortion surrounding the metal center is additional confirmation that Mn has indeed replaced Cu (Cu^{II} is Jahn−Teller distorted) and is also responsible for the transition to a higher symmetry space group, from monoclinic $C2/m$ to trigonal $R\bar{3}m$. Large single crystals of phases with low ($x \leq 0.1$) or high ($x \geq 0.9$) concentration of copper can also be grown and analyzed by single crystal X-ray diffraction (SCXRD). However, because of the similar electron densities of Mn and Cu, the two metals cannot be unequivocally distinguished from each other, and the difference in unit cell parameters turned out to be negligible in this low-concentration regimen. While we were unable to use SCXRD for materials with a combination of metals, we used Rietveld refinement to corroborate the structure of the entire family of materials. We used the Mn-only and the previously reported Cu-only structure[5] as a starting base for Rietveld analysis of the microcrystalline samples (see SI, Table S5 and Figure S2). As expected according to Vegard's law,[14] a shrinkage to the unit cell volume was observed with the incorporation of Cu (Figure S3). The manganese-rich phases ($x < \sim 0.4$) fitted to a trigonal phase, whereas the Cu-rich phases ($x > \sim 0.6$) fitted better to a monoclinic phase. Lastly, the intermediate Mn:Cu ratios ($0.4 \leq x \leq 0.6$) were best described as a disordered phase or a combination of both phases (see SI for details). This behavior is a direct consequence of the difference of the distorted and undistorted geometry around the metal centers, where at high Mn concentrations (Mn > 70%, $x > 0.3$), copper is forced into an almost perfect octahedral environment to adopt a trigonal phase. It is noteworthy that forcing Jahn−Teller active metals into a perfect (or almost perfect) geometry can have interesting effects in the optoelectronic and magnetic properties of materials, as demonstrated previously in oxide and halide perovskites.[13,15,16]

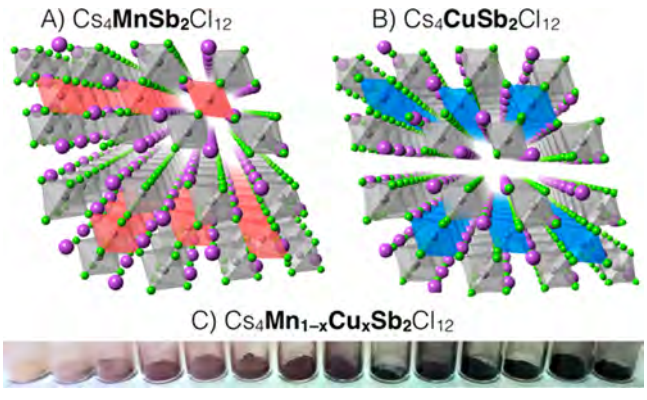

Figure 1. Panels A and B show the crystal structures of $Cs_4MnSb_2Cl_{12}$ and $Cs_4CuSb_2Cl_{12}$, respectively. Cl and Cs atoms are depicted as green and purple spheres, respectively; Sb, Mn, and Cu coordination polyhedra are shown in gray, pink, and blue, respectively. Panel C shows a picture of vials containing microcrystalline $Cs_4Mn_{1-x}Cu_xSb_2Cl_{12}$ samples with x values of 0.0, 0.002, 0.005, 0.02, 0.03, 0.05, 0.1, 0.2, 0.3, 0.4, 0.5, 0.6, 0.8, and 1.0 from left to right, respectively.

Importantly, and similarly to $Cs_4CuSb_2Cl_{12}$, this family of materials have excellent stability, with thermal decompositions well above 200 °C and no observable phase transition from −100 to 200 °C. Further, they also show excellent stability toward humidity, with no apparent decomposition when exposed to 50% relative humidity for up to 26 days (see SI, Figures S6 and S7).

Optical Properties. The Mn-only compound is a light pink microcrystalline powder (Figure 1C). Upon incorporation of small amounts of copper, the solids become purple and turn darker as the concentration of copper increases, until they become black when approximately 40% manganese has been replaced by copper (x = 0.4, Figure 1C).

According to their absorption spectra (Tauc plots, Figures 2B and S8) and DFT calculations (Figures 3 and S13), all compounds have a direct bandgap regardless of copper content. The optical bandgap of the Mn-only and Cu-only materials are 3.0 and 1.0 eV, respectively. For the mixed-metal materials, there is a nonlinear change in bandgap with respect to copper content. First, the bandgap rapidly decreases upon incorporation of small amounts of copper (Figure 2B). Even at x = 0.1, the bandgap drastically decreases from 3.0 to 1.7 eV, which shows that even at small concentrations, copper exerts an important effect on the electronic structure of this family of materials. Similar effects have been observed when doping manganese layer perovskites with small amounts of copper,[13] or upon doping the double perovskite: $Cs_2AgBiBr_6$ with Tl,[17] although not to the extent observed herein.

DOI: 10.1021/acs.chemmater.8b02099
Chem. Mater. 2018, 30, 5315−5321

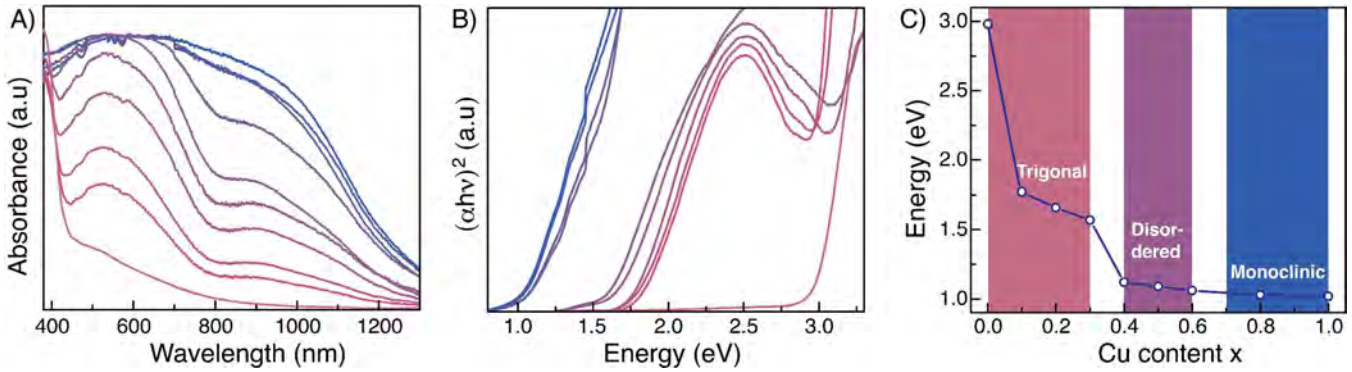

Figure 2. (A) Room-temperature absorbance spectra of $Cs_4Mn_{1-x}Cu_xSb_2Cl_{12}$; from top (blue) to bottom (pink): x = 1.0, 0.8, 0.6, 0.5, 0.3, 0.2, 0.1,0.05. 0.01, and 0.0 (B) Tauc plots of $Cs_4Mn_{1-x}Cu_xSb_2Cl_{12}$; from left (blue) to right (pink): x = 1.0, 0.8, 0.6, 0.5,0.3, 0.2, 0.1, 0.05, 0.01, and 0.0. Note that concentrations of Cu smaller than 5% (x = 0.05) are better described as dopants, and as such, Tauc plots of these materials are only shown for comparison purposes. (C) Optical bandgaps for $Cs_4Mn_{1-x}Cu_xSb_2Cl_{12}$ as a function of copper concentration. The pink, purple, and blue shaded areas highlight the crystalline phases obtained for a given composition.

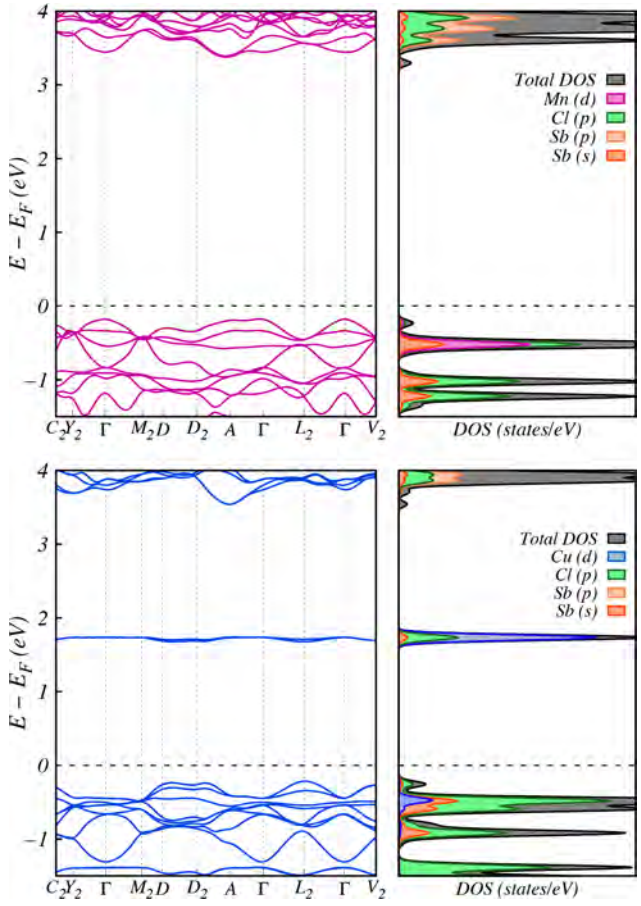

Figure 3. DFT-calculated band structure diagram, total density of states, and partial density of states (DOS/pDOS) of $Cs_4MnSb_2Cl_{12}$ (top) and $Cs_4CuSb_2Cl_{12}$ (bottom).

From x = 0.1 to 0.30, the decrease in the bandgap shows a linear behavior; after that, there is another dip in the bandgap and again, an inverse linear behavior with a smaller slope (Figure 2C). This behavior can be associated with the change in the crystalline phase of the materials, which is indicative of the geometry and electronic environment of the transition metal centers (Figure 1B). Interestingly, the bandgap of the materials with both, copper and manganese, ranges from 1.7 to 1.0 eV, which suggest that this materials have narrow enough bandgaps for absorbing visible and near-infrared light and can, therefore, absorb light in the highest efficiency bandgap range for single absorber solar cells according to the Shockley–Queisser model.[18] Furthermore, we note that this tunable range is significantly larger than the range observed in tin and lead halide perovskites.[1]

While at very small x values (x < 0.05), copper atoms can effectively be considered dopants, the effect on light absorption is evident from their color (Figure 1C), with apparent bandgaps of 1.8–1.7 eV, which are again, significantly lower than the Mn-only bandgap of 3.0 eV. This can be attributed to the formation of midgap states generated by unoccupied copper orbitals. These midgap states are likely to be well above the top of the valence band (VB) and significantly apart from the bulk of the conduction band (CB). At higher x values ($x \geq$ 0.1), in the solid solution regimen, an alternative way to understand the drastic change in bandgap upon copper incorporation, is that Cu introduces new empty midgap states (that are mainly Cu-d in character), where the new states are located significantly apart from both, the VB and the CB. This explanation is consistent with our DFT calculations (vide infra) and could also explain why materials with low copper contents (x < 0.5) show significant subgap absorption as the formation of narrow midgap states that are separated from both, the CB and VB, may allow for a subsequent transition from the midgap state to the bulk of the CB. At greater copper concentrations (x > 0.5) the midgap bands broadens until it fully merges with the CB.

Last, photoluminescence (PL) of these materials was only observed for the Mn-only material (x = 0), which shows strong PL at 605 nm. All other samples did not show significant luminescence up to 900 nm (Figure S9). The photoluminescence observed for the Mn-only is attributed to the transition from the $^4T_1$ to the $^6A_1$ levels in Mn^{2+} atoms, as observed previously in related halide perovskites.[19,20]

DFT Calculations. To better understand the effect of manganese and copper in the electronic structure of these materials, we performed electronic structure calculations for $Cs_4MnSb_2Cl_{12}$ and $Cs_4CuSb_2Cl_{12}$ using density functional theory (DFT) at the HSE06 level.[21] To accurately describe both compounds is necessary to account for their magnetic properties. Accordingly, we explored different spin configurations, namely, one paramagnetic (PM), one ferromagnetic

DOI: 10.1021/acs.chemmater.8b02099
Chem. Mater. 2018, 30, 5315–5321

(FM) and three possible antiferromagnetic configurations (AFM I, II, and III, Figure S10).

Based on the energetics and in agreement with reported calculations[22] and our own magnetic studies (see below), the AFM III structure is the one that best describes both structures ($Cs_4MnSb_2Cl_{12}$ and $Cs_4CuSb_2Cl_{12}$). In this structure, the layers of $[MCl_6]$ (M = Mn or Cu) octahedra are parallel to the $(001)_p$ planes referred to the primitive lattice vectors, or to $(111)_c$ planes referred to pseudocubic axes (see Figure S11 with the pseudocubic cell). The AFM III structure has intralayer antiferromagnetism, with alternating spin polarization along the $[100]_p$ and $[110]_p$ directions and constant spin polarization along the $[010]_p$. These correspond to the pseudocubic system directions $[\bar{1}01]_c$, $[0\bar{1}1]_c$ and $[1\bar{1}0]_c$, respectively. The Cu−Cu distance is smaller along the $[110]_p$ direction (7.33 Å) than along the other two directions (7.47 Å), due to the Jahn−Teller distorted $[CuCl_6]$ octahedra. In contrast, the Mn−Mn distances are all equal (7.483 Å).

Our calculations resulted in almost direct transitions for both, the Mn-only and Cu-only materials with calculated bandgaps values of 3.6 and 1.9 eV, respectively, in decent agreement with our experimental results. While the bandgap is not strictly direct for either the Mn-only, or the Cu-only material, they are only 22 and 5 meV far from this, which for most practical applications (at room temperature) is negligible and is well below the experimental and computational resolution. The calculated density of states (DOS) of the Mn- and Cu-only materials (Figure 3) show significant differences that allows us to understand the large bandgap differences between these two materials. The most significant difference is that the Mn d-orbitals do not contribute significantly to the top of the valence band and only slightly to the bottom of the conduction band, whereas Cu d antibonding orbitals generate a new band located at the bottom of the conduction band, thereby reducing the bandgap. This observation also could explain the appearance of midgap states in the materials with lower Cu content. Similar behavior, where antibonding Cu-d orbitals generates new bands has been reported for copper halide perovskites.[23] In other words, while in the Mn-only perovskite, the bandgap can be assigned to transitions between Cl-p to Sb-p, and in the Cu-only perovskite, this transition is mainly Cl-p to Cu-d in character.

Electronic Structure. To probe our hypothesis and aiming to obtain the atomistic description of the electronic structure evolution of the VB and the Mn and Cu unoccupied 3d states in this family of perovskites, we performed a combination of valence band−X-ray photoelectron spectroscopy (VB−XPS) and synchrotron based soft X-ray absorption (XAS) and emission (XES) spectroscopies at the Mn and Cu Mn $L_{2,3}$ edges for the representative $x = 0$ (Mn-only), 1 (Cu-only), and 0.5 (Cu:Mn, 50:50) samples. VB-XPS and L_α XES probe the total and partial 3d−4s occupied DOS of the metals, respectively. On the other hand, XAS at the Mn and Cu $L_{2,3}$ edges provides information on the Cu and Mn 3d unoccupied states (not the DOS), their oxidation state and the local environment surrounding these cations.[24] The XAS spectra were acquired in total electron (TEY) and total fluorescence (TFY) yield modes. While the first probes surface states, the latter is more bulk sensitive (see SI for details). Hence by analyzing our VB-XPS and XES spectra in the light of our DFT calculations, combined with Cu and Mn $L_{2,3}$ XAS spectra interpreted with atomic-multiplet-calculations (see SI for details), it is possible to obtain key information on the effect of metal alloying in the electronic structure of our perovskites.

The experimental and calculated $L_{2,3}$ XAS spectra for Mn ($x = 0$ and $x = 0.5$) shows two groups of signals that correspond to $2p_{1/2}$ (L_2) and $2p_{3/2}$ (L_3) transitions into $3d_{3/2}$ and $3d_{5/2}$ atomic states (Figure 4A). We observe that the Mn $L_{2,3}$ XAS

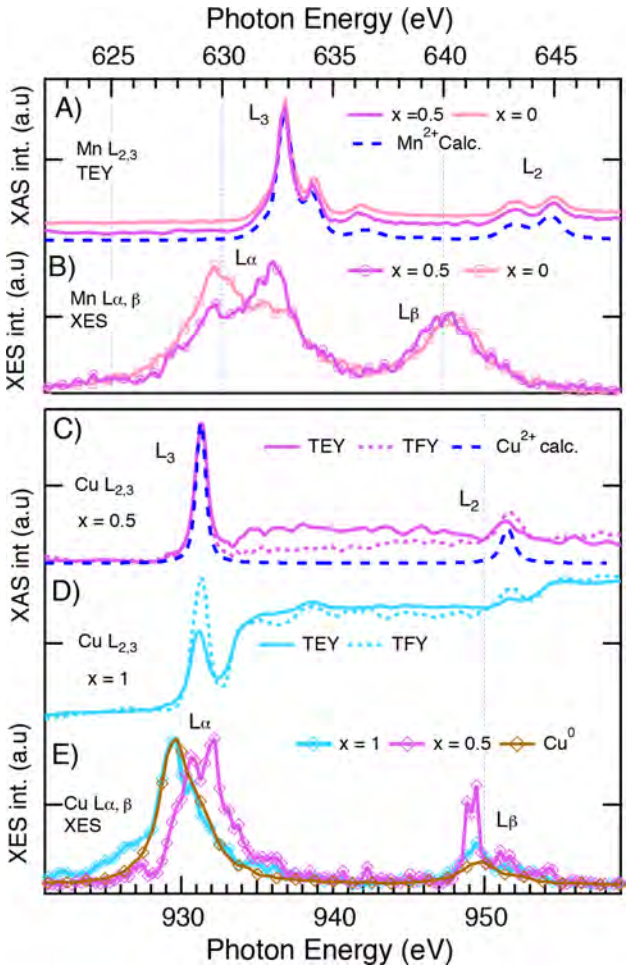

Figure 4. Top panel shows (A) Mn $L_{2,3}$ XAS and (B) XES spectra for $x = 0$ and $x = 0.5$ perovskites. Bottom panel: (C) and (D) Cu $L_{2,3}$ XAS spectra in TEY (solid lines) and TFY (dashed lines), and (E) Cu $L_{\alpha,\beta}$ XES spectra for $x = 0.5$ and $x = 1$ perovskites. Calculated (a) Mn^{2+} and (C) Cu^{2+} $L_{2,3}$ XAS and (E) experimental Cu-foil $L_{\alpha,\beta}$ XES spectra, are indicated by dark-blue-dashed and brown-solid-rumble lines, respectively.

spectra for the $x = 0$ and $x = 0.5$ perovskites are identical. According to our atomic-multiplet calculations, they correspond to Mn^{2+} sites embedded in an almost perfect octahedral environment (see SI for details). Interestingly, while the unoccupied Mn 3d states do not display changes with increasing Cu content, the Mn 3d,4s occupied states, as measured by the Mn L XES spectra, display asymmetric spectral features in the sensitive L_α line (Figure 4B).

Contrary to the observed behavior for Mn, in the case of Cu, the experimental and calculated Cu^{2+} $L_{2,3}$ XAS spectra show significant differences between the spectra for $x = 0.5$ and $x = 1.0$ (Figure 4C−E). For $x = 0.5$, we observe a broad signal between L_2 and L_3 that displays more spectral weight in the TEY (surface) spectrum than in the TFY (bulk) spectrum. As we will show, this broad feature can be attributed to certain

DOI: 10.1021/acs.chemmater.8b02099
Chem. Mater. 2018, 30, 5315−5321

delocalized metallic-like character in the Cu sites. For x = 1 (Figure 4D), the Cu $L_{2,3}$ XAS spectra display a sharp "pre-edge" feature (ca. 931 eV), a small feature. (ca. 952 eV) and two steps (at ca. 935 and 955 eV). The "pre-edge" and the small feature near 952 eV nicely align with the L_3 and L_2 edges in the Cu^{2+} spectra (x = 0.5). On the other hand, the steps resemble those displayed by the Cu $L_{2,3}$ XAS spectra of Cu_2O and Cu-foil (Figure S14). Hence, we can say that while there is clear Cu^{2+} character in both perovskites (particularly in the x = 0.5), there is also a marked metallic-like delocalized character in Cu for the x = 1 perovskite. This behavior seems to be inherent to the samples, since the metallic-like character is more pronounced in the surface (TEY) as compared with the bulk (TFY) of the samples, a quite unusual observation since typically surface states tend to be more oxidized than bulk states. In Figure 4E, the Cu $L_{\alpha,\beta}$ XES spectrum of the x = 0.5 sample shows that the L_α line has more spectral weight toward higher energies than the Cu-only sample. We also notice that the x = 0.5 sample has an unusual intense low energy shoulder in the L_β line and that the XES spectrum of metallic Cu-foil looks more similar to that from the x = 1 perovskite. Previous investigations on the L_α/L_β ratio in varied Cu containing systems established that generally L_α/L_β decreases as the oxidation state of copper increases.[25] The calculated L_α/L_β ratios for our samples were 6.2 (Cu foil) > 3.4 (x = 0) > 1.5 (x = 0.5), which is consistent with the XAS results in the sense that the x = 0.5 sample is mostly Cu^{2+}, while the Cu-only sample exhibits a mixed Cu^{2+}- metallic-like character. Given that the Mn and Cu L_α lines are proportional to the Mn and Cu 3d,4s partial DOS, we can infer that their shoulders are hybridization features. For both metals, we observe an enhancement of the high energy shoulder for x = 0.5 while the low energy shoulders gain spectral weight in the x = 0 and x = 1 extremes of the series, suggesting that the top of the valence band in the x = 0.5 perovskite may have important contribution from transition metal 3d−4s occupied states.

To address the origin of such structures, we combined our XES results with VB-XPS and our calculated DOS. Figure 5 shows the calculated DOS, VB-XPS, XES, and XAS (Cu L_3) spectra aligned based in the energy alignment through hybridization (EATH) method.[26] The energy scale is that from the band structure calculations. Details of the EATH procedure and the VB-XPS spectra beyond −7 eV can be found in the SI. In the Mn-only VB-XPS spectrum (Figure 5B), we observe an asymmetric band at about −2 eV, which seems to be formed by three peaks. These peaks are present on the VB-XPS spectra of the three samples (indicated by vertical solid bars in Figure 5B, C and E). As we increase Cu content, from the x = 0.5 to the Cu-only perovskite, the VB slightly broadens and for x = 1 a new broad state appears below −4 eV resulting in a 2.5 eV broader VB. As a consequence of this broadening, the sharp Cs 5p states at −7 eV in Figure 5B,C are pushed toward more negative energies by approximately the same 2.5 eV in the Cu-only sample (Figures S15 and S17). This new state centered at ca. −5 eV is directly aligned under the Cu L_α line (Figure 5D,E and S17), which indicates that it is related to Cu 3d,4s states.

The agreement between our XAS/XES results and DFT calculations is satisfactory, although our calculations underestimate the spectral weight toward the Fermi level in both materials. According to these, we can also see that the Cl p states contribute the most to the DOS in the VB region. On the other hand, for the Cu-only and Mn-only samples the

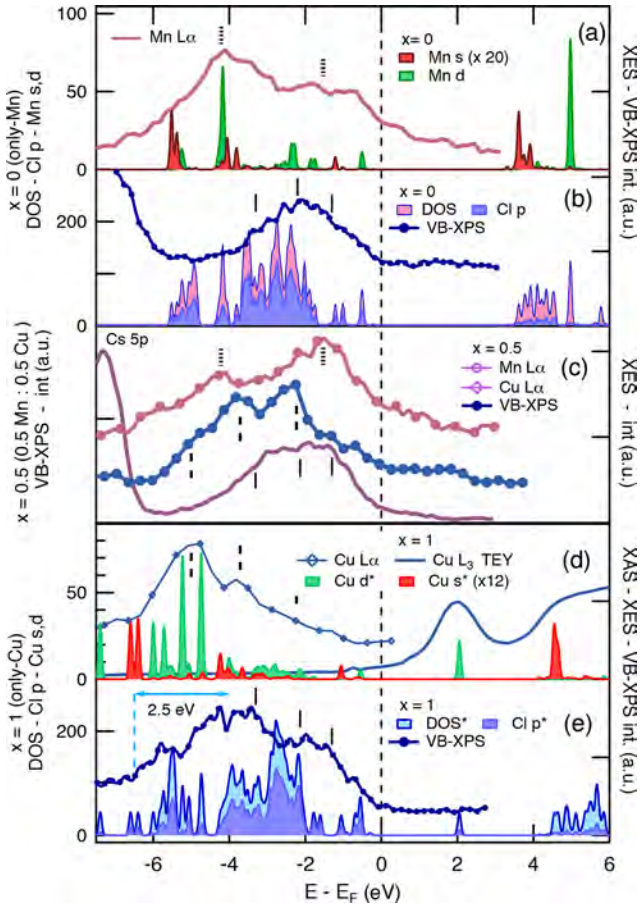

Figure 5. Valence band−X-ray photoelectron spectroscopy (VB−XPS), soft X-ray emission (XES), and absorption (XAS) spectroscopies vs DFT-calculated density of states for the representative x = 0 (A and B), 0.5 (C), and 1.0 (D and E) samples. The * marks in the DOS at the lower panel indicate that the energy axis was multiplied by a factor of 1.17.

calculated 3d and 4s partial DOS are more prominent toward more negative energies (Figure 5B and 5D). This is nicely captured by both Mn and Cu L_α lines as their spectral weight is concentrated toward more negative energies. This suggests, in agreement with the calculation, that the VB top of the Cu-only and only−Mn samples has mostly Cl 2p character, once again, in good agreement with our calculations. On the other hand, the situation is possibly reversed in the x = 0.5 perovskite, where for both Cu and Mn, the experimental 3d−4s partial DOS increase its weight toward the Fermi level, for both, Cu and Mn (Figure 5C). It is worth mentioning that all the structures observed in the VB-XPS and XES spectra find a one to one correspondence between each other as indicated by the solid, dashed and dotted bars accompanying the spectra, which validates our spectral alignment. In terms of the unoccupied states, we included the Cu L_3 XAS spectrum for the Cu-only perovskite. We did so, because in this case the calculation provides an alternative but consistent understanding the "pre-edge" Cu^{2+} peak and the first step observed in the spectrum. In this scheme, the first "pre-edge" structure has 3d (green) character while the step has an itinerant (delocalized) 4s (red) character (Figures S17 and S18).

From this analysis, we can say that in the Mn-only and Cu-only materials, the top of the VB is mostly composed by Cl p states and that increasing Cu content broadens the VB by

DOI: 10.1021/acs.chemmater.8b02099
Chem. Mater. 2018, 30, 5315−5321

about 2.5 eV shifting the Cs 5p peak toward more negative energies. In addition, in agreement with the calculations, while the bandgap is between Cl p−Sb p states in the Mn-only sample, it seems to be between Cl p−Cu d states in the Cu-only sample (Figure 5D,E). On the other hand, for the $x = 0.5$ sample, the top of the VB has an increased Mn d character as compared with the Mn-only sample (Figure 5C). A detailed analysis of our VB-XPS, XAS, XES, and resonant inelastic X-ray (RIXS) experiments will be reported separately shortly.

Magnetism. The presence of first row transition metals with unpaired electrons in the $Cs_4Mn_{1-x}Cu_xSb_2Cl_{12}$ family prompted us to study its magnetic behavior. First, the product of magnetic susceptibility and temperature (χT) of $Cs_4MnSb_2Cl_{12}$ clearly shows an antiferromagnetic behavior that follows the Curie−Weiss Law with values of $\theta = -6.9$ K and C = 4.14 emu/mol. The magnetic behavior observed for $Cs_4MnSb_2Cl_{12}$ is additional validation of the electronic structure determined by our DFT calculations. On the other extreme, $Cs_4CuSb_2Cl_{12}$ shows an antiferromagnetic interaction between Cu^{2+} centers. Importantly, in this case, the magnetic response as the temperature decreases does not follow the Curie−Weiss law, and a linear decay of χT as the temperature drops can be observed, which is best described by temperature-independent paramagnetism (TIP) with a value of 1.05×10^3 emu mol^{-1} K. The TIP behavior on the Cu-only perovskite is indicative of delocalization of thermo-excited charge carriers, which is also consistent with the Cu L_3 XAS spectra and the metallic-like character observed by the L_α/L_β ratio and the previously reported conductivity for this material, which was reported to be higher than expected for a 2D material.[5] Similar Pauli paramagnetism behavior has been observed for semiconductors based on coordination[27] and organic polymers.[28]

The distinct magnetic behavior of $Cs_4MnSb_2Cl_{12}$ and $Cs_4CuSb_2Cl_{12}$ phases allows modulation of the antiferromagnetic behavior for the mixed-metal phases: $Cs_4Mn_{1-x}Cu_xSb_2Cl_{12}$. (Figure 6). As x values increases, the

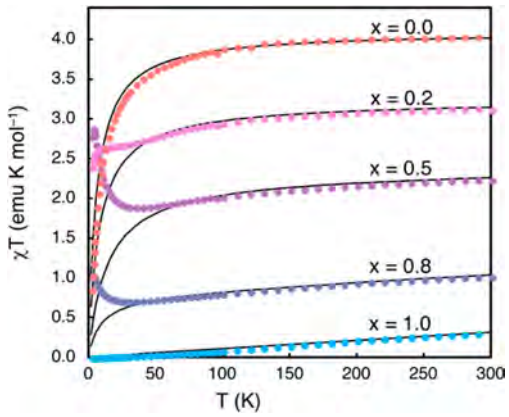

Figure 6. Temperature dependence of the magnetic susceptibility-temperature (χT) product for $Cs_4Mn_{1-x}Cu_xSb_2Cl_{12}$ (from top to bottom $x = 0.0, 0.2, 0.5, 0.8, 1.0$). Solid lines represent the best fit of the data.

TIP value increases and the Pauli paramagnetism state gradually increases due to rising concentrations of movable charge carriers (Table S8). The data considerably deviates from the fitting model of Curie−Weiss law combined with TIP at temperatures below 50 K for intermediate compositions (x = 0.8, 0.5, 0.2), but using the Néel's hyperbolic equation did not result in a better fitting. A magnetic phase transition at temperatures below 50 K was suspected for the intermediate compositions, but there is no bifurcation between FC and ZFC data (Figures S18−S20), which indicates the absence of ferrimagnetic ordering in the 50−2 K temperature range.

CONCLUSIONS

In conclusion, we have demonstrated that by means of metal doping or alloying, it is possible to modulate the electronic structure of this family of materials, which in turns leads to unprecedented ability to control their optical properties, and for the first time, we show the ability to systematically tune the magnetic properties of halide perovskites. Furthermore, this study shows that ⟨111⟩ layered perovskites offer a rich chemical space wherein other metals, or a combination of them, can be incorporated to give rise to properties that were previously not possible in halide perovskites. Apart from their possible application in photovoltaics, we hope that the rich chemistry and properties shown in this study incites the community to explore other possible applications and properties of ⟨111⟩ layered perovskites such as thermoelectric or magneto-optic properties.

ASSOCIATED CONTENT

Supporting Information

The Supporting Information is available free of charge on the ACS Publications website at DOI: 10.1021/acs.chemmater.8b02099.

Detailed experimental procedures, crystallographic data, and computational details (PDF)

X-ray crystallographic file of $Cs_4MnSb_2Cl_{12}$ (CIF)

AUTHOR INFORMATION

Corresponding Authors

*E-mail: paulol@ifuap.buap.mx.

*E-mail: diego.solis@unam.mx.

ORCID

Diego Solis-Ibarra: 0000-0002-2486-0967

Author Contributions

▲(B.V., R.T.-C.) These authors contributed equally.

Funding

The authors thank funding from PAPIIT IA202418 and CONACYT FC-2015−2/829. B.V. and R.T.-C. acknowledge the support from CONACYT scholarships. P.O.-V. would like to acknowledge VIEP-BUAP and Red Temática de Usuarios de Luz Sincrotrón (REDTULS) CONACYT for traveling and lodging expenses support to collect X-ray data at the ALS. The work of P.O.-V. at Puebla, Mexico is supported by SEP (511-6/17-8017) PTC-553 and VIEP-BUAP (OLVP-exc17). This research used resources of the Advanced Light Source, which is a DOE Office of Science User Facility under contract no. DE-AC02-05CH11231. E.M.-P. and R.T.-C. acknowledge support from FONDECYT Grant No. 1171807. Powered@NLHPC. This research was partially supported by the supercomputing infrastructure of the NLHPC (ECM-02). H.X. and K.R.D. were supported by the Department of Energy, Basic Energy Sciences, Material Sciences Division under grant number DE-FG02-02ER45999 and the Robert A. Welch Foundation (A-1449). N.L. is grateful for financial support from the Secretariat of Public Education (grant UAEMOR-PTC-388).

DOI: 10.1021/acs.chemmater.8b02099
Chem. Mater. 2018, 30, 5315−5321

Notes

The authors declare no competing financial interest.

■ ACKNOWLEDGMENTS

We acknowledge the support of E. Pérez-Gutiérrez, A. Tejeda, C. Ramos, L. Huerta, E. Morales, A. Vivas, A. Pompa, C. González, M. Canseco and M. Olmos.

■ REFERENCES

(1) Stoumpos, C. C.; Kanatzidis, M. G. The Renaissance of Halide Perovskites and Their Evolution as Emerging Semiconductors. *Acc. Chem. Res.* **2015**, *48*, 2791−2802.
(2) Saparov, B.; Mitzi, D. B. Organic−Inorganic Perovskites: Structural Versatility for Functional Materials Design. *Chem. Rev.* **2016**, *116*, 4558−4596.
(3) Slavney, A. H.; Smaha, R. W.; Smith, I. C.; Jaffe, A.; Umeyama, D.; Karunadasa, H. I. Chemical Approaches to Addressing the Instability and Toxicity of Lead−Halide Perovskite Absorbers. *Inorg. Chem.* **2017**, *56*, 46−55.
(4) Zhang, F.; Zhong, H.; Chen, C.; Wu, X.-G.; Hu, X.; Huang, H.; Han, J.; Zou, B.; Dong, Y. Brightly Luminescent and Color-Tunable Colloidal $CH_3NH_3PbX_3$(X = Br, I, Cl) Quantum Dots: Potential Alternatives for Display Technology. *ACS Nano* **2015**, *9*, 4533−4542.
(5) Vargas, B.; Ramos, E.; Pérez-Gutiérrez, E.; Alonso, J. C.; Solis-Ibarra, D. A Direct Bandgap Copper−Antimony Halide Perovskite. *J. Am. Chem. Soc.* **2017**, *139*, 9116−9119.
(6) Saparov, B.; Hong, F.; Sun, J.-P.; Duan, H.-S.; Meng, W.; Cameron, S.; Hill, I. G.; Yan, Y.; Mitzi, D. B. Thin-Film Preparation and Characterization of $Cs_3Sb_2I_9$: A Lead-Free Layered Perovskite Semiconductor. *Chem. Mater.* **2015**, *27*, 5622−5632.
(7) Tang, G.; Xiao, Z.; Hosono, H.; Kamiya, T.; Fang, D.; Hong, J. J. Layered Halide Double Perovskites $Cs_{3+n}M(II)_nSb_2X_{9+3n}$ (M = Sn, Ge) for Photovoltaic Applications. *J. Phys. Chem. Lett.* **2018**, *9*, 43−48.
(8) Hoye, R. L. Z.; Brandt, R. E.; Osherov, A.; Stevanović, V.; Stranks, S. D.; Wilson, M. W. B.; Kim, H.; Akey, A. J.; Perkins, J. D.; Kurchin, R. C.; Poindexter, J. R.; Wang, E. N.; Bawendi, M. G.; Bulović, V.; Buonassisi, T. Methylammonium Bismuth Iodide as a Lead-Free, Stable Hybrid Organic−Inorganic Solar Absorber. *Chem. - Eur. J.* **2016**, *22*, 2605−2610.
(9) Lehner, A. J.; Fabini, D. H.; Evans, H. A.; Hébert, C.-A.; Smock, S. R.; Hu, J.; Wang, H.; Zwanziger, J. W.; Chabinyc, M. L.; Seshadri, R. Crystal and Electronic Structures of Complex Bismuth Iodides $A_3Bi_2I_9$ (A= K, Rb, Cs) Related to Perovskite: Aiding the Rational Design of Photovoltaics. *Chem. Mater.* **2015**, *27*, 7137−7148.
(10) Singh, A.; Boopathi, K. M.; Mohapatra, A.; Chen, Y. F.; Li, G.; Chu, C.-W. Photovoltaic Performance of Vapor-Assisted Solution-Processed Layer Polymorph of $Cs_3Sb_2I_9$. *ACS Appl. Mater. Interfaces* **2018**, *10*, 2566−2573.
(11) McCall, K. M.; Stoumpos, C. C.; Kostina, S. S.; Kanatzidis, M. G.; Wessels, B. W. Strong Electron−Phonon Coupling and Self-Trapped Excitons in the Defect Halide Perovskites $A_3M_2I_9$ (A = Cs, Rb; M = Bi, Sb). *Chem. Mater.* **2017**, *29*, 4129−4145.
(12) Hebig, J.-C.; Kühn, I.; Flohre, J.; Kirchartz, T. Optoelectronic Properties of $(CH_3NH_3)_3Sb_2I_9$ Thin Films for Photovoltaic Applications. *ACS Energy Lett.* **2016**, *1*, 309−314.
(13) Schmid, U.; Guedel, H. U.; Willett, R. D. Origin of the red color in copper(II)-doped ethylenediammonium tetrachloromanganate(II). *Inorg. Chem.* **1982**, *21*, 2977−2982.
(14) Vegard, L. Die Konstitution der Mischkristalle und die Raumfüllung der Atome. *Eur. Phys. J. A* **1921**, *5*, 17−26.
(15) Huang, H. Y.; Chen, Z. Y.; Wang, R. P.; de Groot, F. M. F.; Wu, W. B.; Okamoto, J.; Chainani, A.; Singh, A.; Li, Z. Y.; Zhou, J. S.; Jeng, H. T.; Guo, G. Y.; Park, J.-G.; Tjeng, L. H.; Chen, C. T.; Huang, D. J. Jahn-Teller distortion driven magnetic polarons in magnetite. *Nat. Commun.* **2017**, *8*, 15929.
(16) Kumar, P. S. A.; Joy, P. A.; Date, S. K. Evidence for Jahn - Teller polaron formation and spin-cluster-assisted variable-range-hopping conduction in $La_{0.7}Ca_{0.3}MnO_3$. *J. Phys.: Condens. Matter* **1998**, *10*, L269−L275.
(17) Slavney, A. H.; Leppert, L.; Bartesaghi, D.; Gold-Parker, A.; Toney, M. F.; Savenije, T. J.; Neaton, J. B.; Karunadasa, H. I. Defect-Induced Band-Edge Reconstruction of a Bismuth-Halide Double Perovskite for Visible-Light Absorption. *J. Am. Chem. Soc.* **2017**, *139*, 5015−5018.
(18) Rühle, S. Tabulated values of the Shockley−Queisser limit for single junction solar cells. *Sol. Energy* **2016**, *130*, 139−147.
(19) Liu, W.; Lin, Q.; Li, H.; Wu, K.; Robel, I.; Pietryga, J. M.; Klimov, V. I. Mn^{2+}-Doped Lead Halide Perovskite Nanocrystals with Dual-Color Emission Controlled by Halide Content. *J. Am. Chem. Soc.* **2016**, *138*, 14954−14961.
(20) Song, P.; Zhang, C. M.; Zhu, P. F. Transition metal and rare earth quad-doped photovoltaic phosphate glasses toward raising a-SiC:H solar cell performance. *J. Opt.* **2016**, *18*, 015901−8.
(21) Krukau, A. V.; Vydrov, O. A.; Izmaylov, A. F.; Scuseria, G. E. Influence of the exchange screening parameter on the performance of screened hybrid functionals. *J. Chem. Phys.* **2006**, *125*, 224106.
(22) Wang, X.; Meng, W.; Xiao, Z.; Wang, J.; Mitzi, D.; Yan, Y. First-Principles Understanding of the Electronic Band Structure of Copper-Antimony Halide Perovskite: The Effect of Magnetic Ordering. 2017, arXiv:1707.09539 [cond-mat.mtrl-sci]. arXiv.org e-Print archive. https://arxiv.org/abs/1707.09539.
(23) Cortecchia, D.; Dewi, H. A.; Yin, J.; Bruno, A.; Chen, S.; Baikie, T.; Boix, P. P.; Grätzel, M.; Mhaisalkar, S.; Soci, C.; Mathews, N. Lead-Free $MA_2CuCl_xBr_{4-x}$ Hybrid Perovskites. *Inorg. Chem.* **2016**, *55*, 1044−1052.
(24) de Groot, F.; Kotani, A. *Core Level Spectroscopy of Solids*; CRC Press: Boca Raton, FL, 2008.
(25) Kawai, J.; Nakajima, K.; Gohshi, Y. Copper L_β/L_α X-ray emission intensity ratio of copper compounds and alloys. *Spectrochim. Acta, Part B* **1993**, *48*, 1281.
(26) Olalde-Velasco, P.; Jiménez-Mier, J.; Denlinger, J. D.; Hussain, Z.; Yang, W. L. Direct probe of Mott-Hubbard to charge-transfer insulator transition and electronic structure evolution in transition-metal systems. *Phys. Rev. B: Condens. Matter Mater. Phys.* **2011**, *83*, 241102.
(27) An, W.; Aulakh, D.; Zhang, X.; Verdegaal, W.; Dunbar, K. R.; Wriedt, M. Switching of Adsorption Properties in a Zwitterionic Metal−Organic Framework Triggered by Photogenerated Radical Triplets. *Chem. Mater.* **2016**, *28*, 7825−7832.
(28) Rizzuto, F. J.; Hua, C.; Chan, B.; Faust, T. B.; Rawal, A.; Leong, C. F.; Hook, J. M.; Kepert, C. J.; D'Alessandro, D. M. The electronic, optical and magnetic consequences of delocalization in multifunctional donor−acceptor organic polymers. *Phys. Chem. Chem. Phys.* **2015**, *17*, 11252−11259.

DOI: 10.1021/acs.chemmater.8b02099
Chem. Mater. 2018, 30, 5315−5321